Colloids with a tunable dipolar interaction: equations of state and order parameters *via* confocal microscopy

Ning Li, Hugh D. Newman, Manuel Valera, Ivan Saika-Voivod and Anand Yethiraj*

Received 20th May 2009, Accepted 5th November 2009
First published as an Advance Article on the web 21st December 2009
DOI: 10.1039/b909953k

Laser scanning confocal microscopy studies were carried out on charged screened colloidal silica microspheres in sedimentation equilibrium in the presence of a tunable external alternating electric field. The external a.c. field controls the averaged dipolar interaction between the silica microspheres. From the equilibrium sedimentation profiles, equations of state were obtained as a function of the dipolar strength and volume fraction. The colloidal fluid at zero field follows the hard-sphere equation of state but with an effective larger hard-sphere diameter. At non-zero fields, the average colloidal fluid isothermal compressibility was obtained as a function of a dipolar strength parameter. We then investigated bond order parameters upon increasing the field, and monitored an orientational order parameter associated with the field dependence of the average orientation of dual-particle bonds. The orientational order parameters were found to be very sensitive measures of anisotropy. The field dependence strongly confirms the use of the point dipolar approximation in this system.

1 Introduction

Colloids with tunable interactions are very promising systems for studying the fundamental physics of the liquid state,[1] crystallization kinetics,[2,3] martensitic transitions[4–6] and kinetic arrest at glass and gel transitions.[7] These studies would benefit greatly from systems where these tunable interactions can be switched on and off instantaneously to provide the equivalent of temperature or pressure quenches in the study of colloidal phase transitions.[8]

One of a few such systems is a colloidal suspension with a tunable dipolar interaction, controllable by the strength of an external (linear or rotating) a.c. electric field.[4–6,9,10] The dipolar interaction is an important driving force for nanoparticle self-organization.[11] Simulations of magnetic dipolar colloids with an additional Lennard-Jones interaction have shown numerous variants (linear aggregates, droplets, columns) of phase separation into regions of higher and lower densities.[12,13] Recent experiments in Brownian dipolar colloids also exhibit an unusual void phase at very low packing ($\varphi < 1\%$).[10] It is important, however, to establish quantitatively the relation between the applied external field and the resultant modulation of the interparticle interaction, especially in light of questions regarding the limitations of the point dipole model.[14] The fluid phase can be used to test quantitatively whether the interaction of two particles in the presence of a sea of other spheres is still effectively captured by the point dipolar approximation (as has been shown in the case of two isolated spheres[15]), and to obtain experimentally the equation of state of dipolar fluids. Thus far this has not been done.

The equilibrium sedimentation profile of colloidal suspensions has been utilized to obtain the colloidal hard-sphere equation of state.[1,16–18] It has also been used to obtain the equation of state for colloid–polymer mixtures.[19] However, while many studies of local dynamics in both hard-sphere colloids as well as colloids with longer-range interactions are carried out using confocal microscopy, *i.e.* in thin cells close to a bounding surface, quantitative tests of colloid thermodynamics (measurement of the equation of state) have been limited to bulk samples. A test of colloid thermodynamics in the realistic case of colloids experiencing external forcing (either bounding surfaces or electric-field-tunable interactions or both) is thus of broad importance.

In this work, we obtain sedimentation profiles for thin colloidal sediments obtained *via* confocal microscopy. We use these sedimentation profiles to obtain the equations of state and isothermal compressibilities for a colloidal suspension as a function of the magnitude of an applied external electric field, *i.e.* as a function of increasing dipolar strength, with the field direction being perpendicular to gravity. In this geometry both the electric field and gravity are simultaneously important. Going beyond the equation of state, we directly calculate an orientational order parameter to shed light on local anisotropy in the fluid state at small fields well below the field strength at which long chains form. From the functional dependence of the order parameter, we conclude that an effective dipolar approximation is quantitatively valid.

The equation of state in bulk systems of screened, charge-stabilized colloids has been shown to exhibit quantitative agreement[18] with the Carnahan–Starling relation which expresses the osmotic pressure in a colloidal suspension at packing fraction φ as $\Pi(\varphi) = nk_BTZ(\varphi)$, where the particle number density n is related to the packing fraction by $\varphi = n(4\pi a^3/3)$ (where a is the particle radius) and $Z(\varphi) = (1 + \varphi + \varphi^2 - \varphi^3)/(1 - \varphi)^3$ is the Carnahan–Starling compressibility factor.[20]

The decrease in osmotic pressure for an increment in vertical position dz in a colloidal sediment is given by $d\Pi = -g\Delta\rho\varphi(z)dz$. Here $\Delta\rho$ is the particle–solvent density mismatch. Integrating this from position z until a height where no more particles are found yields the equation of state:

Department of Physics and Physical Oceanography, Memorial University, St. John's, Newfoundland, Labrador, Canada. E-mail: ayethiraj@mun.ca

$$\Pi(z) = \int_z^\infty g\Delta\rho\varphi(z')dz' \quad (1)$$

One can also calculate the isothermal compressibility

$$\chi_T = k_BT/(\partial\Pi/\partial n)_T \quad (2)$$

For hard spheres, $\chi_T = \dfrac{\partial[\phi Z(\phi)]}{\partial\phi}$ is independent of particle radius a. At low density, $\chi_T = \chi_T^{app}$ is often taken as a constant (although this is not strictly valid) and eqn (2) reduces to $\varphi = \varphi_0 \exp(-\chi_T^{app} z/l_g)$. Here χ_T^{app} is the apparent compressibility in the barometric regime and l_g is the gravitational length defined as $l_g = k_BT/(4/3\pi a^3 g\Delta\rho)$.

More detailed structural information may be obtained at different depths z in the colloidal sediment to detect the presence of the field. We do so by way of an order parameter based on the angle a bond between two particles makes with respect to the field direction.

In what follows we obtain the equation of state (*via* eqn (1)) and the isothermal compressibility (*via* eqn (2)), as well as orientational order parameters, from sedimentation profiles obtained *via* confocal microscopy.

2 Experimental

We prepare our colloidal samples with fluorescent core–non-fluorescent shell silica microspheres (synthesized as by van Blaaderen and Vrij[21]) suspended in a water–dimethyl sulfoxide mixture (15 : 85 in volume for refractive index matching). The diameter of the fluorescent core is 0.46 μm ± 6.9%. The two batches of core–shell spheres have diameters $\sigma = 2a$ of 0.77 μm (3.8% polydispersity) and 1.14 μm (3.4% polydispersity). Sandwich cells were made using 75 μm thick polyethylene terephthalate film as spacers and UV epoxy. A 1 MHz a.c. electric field was generated using a dual-channel function generator and a wide-band amplifier, and the potential between gold electrodes was monitored by a two-channel digital storage oscilloscope. In order to apply linear and rotating fields, gold electrodes were patterned onto the microscope slide (top plate) and the cover slip (bottom plate) of a "sandwich cell" by gold vapor deposition through masks machined with the required geometry. For geometry 1 (linear field), two parallel electrodes were patterned on bottom and top plates. Each electrode on the bottom plate was shorted to the electrode above it on the top plate. Geometry 2, with 4 electrodes on each plate instead of 2 to create two diagonal electrode pairs, was used to achieve a switchable rotary or linear field. For a rotary field, we used a dual channel signal (one 90° phase shifted with respect to the other) and separately connected them to each pair. The instantaneous field direction at the center then rotates at mega-Hertz frequency (the Lissajous figure on the oscilloscope is circular). By switching the phase shift between the two channels from 90 to 0°, we switch from a rotary to linear field in the same colloidal system and switch the anisotropy of the system without altering the energy that might be pumped into the system. The center of the electrodes where no gold is deposited is the place we probe our colloids under external fields using a VisiTech VT-Eye confocal scanner attached to a Nikon inverted microscope and equipped with a 491 nm laser.

3 Equations of state

The equation of state can be extracted from the equilibrium sedimentation profile in a colloidal suspension. Shown in Fig. 1(a) is the evolution of sedimentation profiles (for zero applied field) after a sample is first inverted and placed on the microscope stage. For our systems, the Brownian time ($\tau_B = 6\pi\eta a^3/k_BT$) and the Stokes time ($\tau_S = h/v_s$ where $h \approx 30$ μm is the sediment height and $v_s = (2\Delta\rho g/9\eta)a^2$is the Stokes velocity of a sphere) are roughly 0.5 s and 2 min respectively. For times larger than 15 min, the sedimentation profiles can be seen to approach the equilibrium profile. We typically waited a minimum of 15 min before obtaining equilibrium profiles (on the order of 1000 Brownian and 10 Stokes times).

The sedimentation profile is a sensitive indicator of residual electrostatic effects in a nearly hard-sphere-like charge-stabilized

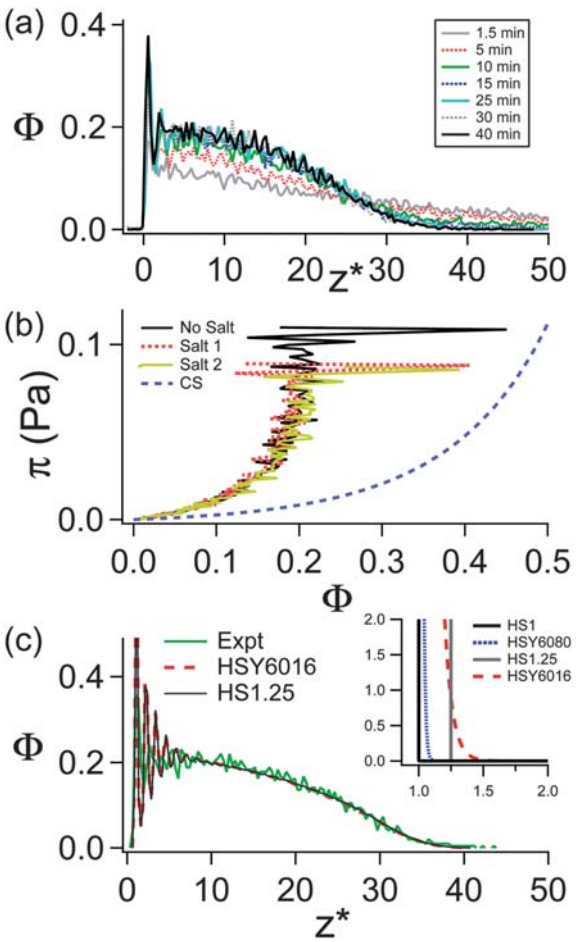

Fig. 1 Quiescent sedimentation profile for $\sigma = 0.77$ μm. (a) Approach to the equilibrium sedimentation profiles. Volume fraction (φ) *vs.* depth (in dimensionless units; $z^* = z/\sigma$, $\sigma = 2a$) as a function of time waited. Steady state equilibrium profiles are achieved after between 15 to 30 min. (b) The equation of state obtained at different ionic strengths ($\kappa\sigma > 15$) are in agreement with each other, but not in agreement with the hard-sphere equation of state. (c) The tail of the sedimentation profile is well fit either by a softer hard-sphere plus Yukawa potential ("HSY6016": $\varepsilon = 60$, $\kappa\sigma = 16$) or an effective hard-sphere approximation ("HS1.25":$\sigma_{eff} = 1.25\sigma$). Inset: However, changing κ^{-1} so that $\kappa\sigma = 80$ ("HSY6080") makes the simulation potential much closer to the hard sphere potential ("HS1"), while the experimental profile is identical to that at $\kappa\sigma = 16$.

colloidal suspension.[22] Fig. 1(a) shows layering oscillations close to the bottom surface (dimensionless height $z^* = z/\sigma = 0$, $\sigma = 2a$ is particle diameter) without crystal formation (consistent with previous work[23]). The equation of state in equilibrium shows significant deviation from the Carnahan–Starling hard-sphere equation of state. Sedimentation profiles at three distinct ionic strengths were obtained—no salt added ("no salt": screening length $\kappa^{-1} = 53 \pm 2$ nm), as well as with (KCl) salt added ("salt 1": $\kappa^{-1} = 50 \pm 2$ nm, and "salt 2": $\kappa^{-1} = 10 \pm 2$ nm). Given that $\kappa\sigma > 10$ for all samples, they are expected to be indistinguishable and to exhibit hard-sphere-like behaviour. The equation of state was then calculated (Fig. 1(b)). All experimental equations of state in Fig. 1(b) are indeed indistinguishable, but at significant deviation from the hard-sphere equation of state (dashed line in Fig. 1(b)).

As shown in Fig. 1(b), there is a steep rise in osmotic pressure at a packing fraction close to 0.2, and at higher pressures the curve oscillates back and forth in φ. This oscillation in local volume fraction is the layering close to the bottom substrate. We verify dynamically that this layering is not truly solid like but fluid like. The rise in osmotic pressure happens at lower packing fraction than for hard spheres (0.49 for hard spheres). The fact that the sedimentation profiles in thin sediments correspond to an equation of state that deviates from the hard-sphere equation of state is remarkable, but consistent with previous observations of extended sedimentation profiles in thin colloidal sediments.[23,24]

To address this discrepancy, we consider the hard-sphere potential with an added Yukawa interaction

$$\frac{u_Y(r)}{k_BT} = \varepsilon\frac{\exp[-\kappa(r-\sigma)]}{r/\sigma} \quad (3)$$

for $r > \sigma$. For $\kappa\sigma = 16$ (as in "salt 1") this potential has a steep rise at $r/\sigma_{\mathrm{eff}} = 1$, with an effective hard-sphere diameter $\sigma_{\mathrm{eff}} > \sigma$ that varies roughly as log ε. Indeed, we obtain a better fit to the fluid part of the sedimentation profile by carrying out simulations[25] of a system of particles under gravity interacting through eqn (3), with $\kappa\sigma = 16$ and varying ε. We use molecular dynamics simulation of 4000 particles in a $20.2\sigma \times 20.2\sigma \times 122\sigma$ cell that is periodic in the xy plane with gravity along the z axis. The areal density ($= 9.8/\sigma^2$) was chosen to match the experimental value. In addition, we carried out simulations of sedimenting hard spheres of fixed mass and buoyant force but varying σ_{eff}. We approximated the discontinuous hard-sphere potential with a Lennard-Jones potential cut at the minimum of the potential $2^{1/6}\sigma$ and shifted up to zero, with $k_BT/\varepsilon_{\mathrm{LJ}} = 1$, ensuring that the bulk equation of state matches the Carnahan–Starling model.† Fig. 1(c) shows that both the Yukawa system with $\varepsilon = 60$ (the dependence on ε is logarithmic) and hard spheres with $\sigma_{\mathrm{eff}} = 1.25$ match fairly well the experimental profile. If we stopped here, we could conclude that a sufficiently large surface charge could produce a hard-sphere-like profile with $\sigma_{eff} > \sigma$ even when the screening length is short.

† Continuous potentials are used to approximate hard spheres; see *e.g.* Voigtmann *et al.*[26] where the authors use a simple power law potential with exponent 36. In our simulations, we confirm that our potential is sufficiently hard-sphere-like by checking that doubling the exponents in our potential results in no significant change in our simulated profiles.

However, if we assume that surface charge will not increase when more salt is added, we can test the above. Plotting the hard-sphere-plus-Yukawa potential for $\varepsilon = 60$ and $\kappa\sigma = 80$, we find that $\sigma_{eff} \approx 1\sigma$ (Fig. 1(c) inset). Therefore, the experiments done with "salt 2" ($\kappa\sigma = 80$) should return the profiles to true hard-sphere profiles. However, experimentally the "salt 2" profiles are indistinguishable from the "salt 1" profiles.

The upshot of this detailed analysis is that we cannot explain the extended sedimentation profiles (*i.e.* $\sigma_{eff} > \sigma$) observed in this study with a simple electrostatic repulsion model. One reason sometimes invoked for such discrepancies is the breakdown of the one-component fluid approach in a sedimented (and therefore spatially heterogeneous) colloidal dispersion; that is, while the colloids (the macro-ions) are sedimented, the counterions are dispersed throughout the solvent, giving rise to poorer charge screening than in the unsedimented dispersion.[16,24] This explanation too seems less likely in the presence of added salt. The main point to be noted is that the equation of state at zero field is robust and can be fit to an effective hard-sphere density profile.

The next experiment was to obtain sedimentation profiles as a function of applied voltage. The dipolar interparticle interaction energy (scaled with respect to k_BT) has the form

$$u_{\mathrm{dipolar}}/k_BT = \frac{\Lambda}{(R/\sigma)^3}\left(\frac{3\cos^2\theta - 1}{2}\right) \quad (4)$$

where a is the particle radius, $\sigma = 2a$, R is the interparticle distance, $E_o = V_o/d$ is the zero-peak electric field amplitude, $\beta = (\varepsilon_p - \varepsilon_f)/(\varepsilon_p + 2\varepsilon_f)$, with ε_f and ε_p being the fluid and particle dielectric constant and Λ is the dipolar strength parameter $\Lambda = \pi\varepsilon_0\varepsilon_f\beta^2a^3E_o^2/2k_BT$. The angle θ is the angle between the line joining particle centres and the field direction. Λ represents the magnitude of the scaled dipolar energy for two touching particles $R = 2a$ and $\theta = 0$ and can be calculated from the applied zero-peak potential difference V_o, the electrode gap of 2 mm, and the particle and solvent properties. The particle volume fraction as a function of height z^* from the bottom was obtained at varying dipolar strengths Λ. Fig. 2(a) shows the volume fraction as a function of z^* for different V_o. It is immediately apparent that the tail of the sedimentation profile becomes steeper and less extended with increasing voltage. From these sedimentation profiles and using eqn (1) we obtain next the equation of state as a function of increasing voltage (Fig. 2(b)). Only curves for $V_o =$ 0, 100 V, 200 V and 300 V are shown, for clarity. At low φ, the applied field induces interactions that reduce both the pressure Π as well as $d\Pi/d\varphi$. These interactions also tend to increase the φ at which the sediment becomes roughly incompressible [the near-vertical slopes in Fig. 2(b)].

Next, we calculated the *apparent* isothermal osmotic compressibility χ_T^{app} (using eqn (2)) by linearly fitting the logarithm of the exponentially decaying (low φ) regime of the sedimentation profile. We obtain $\chi_T^{app} = 0.68$ for $\sigma = 0.77$ μm and $\chi_T^{app} = 0.59$ for $\sigma = 1.14$ μm at zero field. The particle-radius dependence of χ_T^{app} as well as the observation that $\chi_T^{app} < 1$ is indicative of the residual repulsions already noted in Fig. 1(c). As the applied electric field is increased in steps, the apparent compressibility of the fluid χ_T^{app} increases as well (Fig. 2(c)). This too is consistent. It should indeed be energetically more

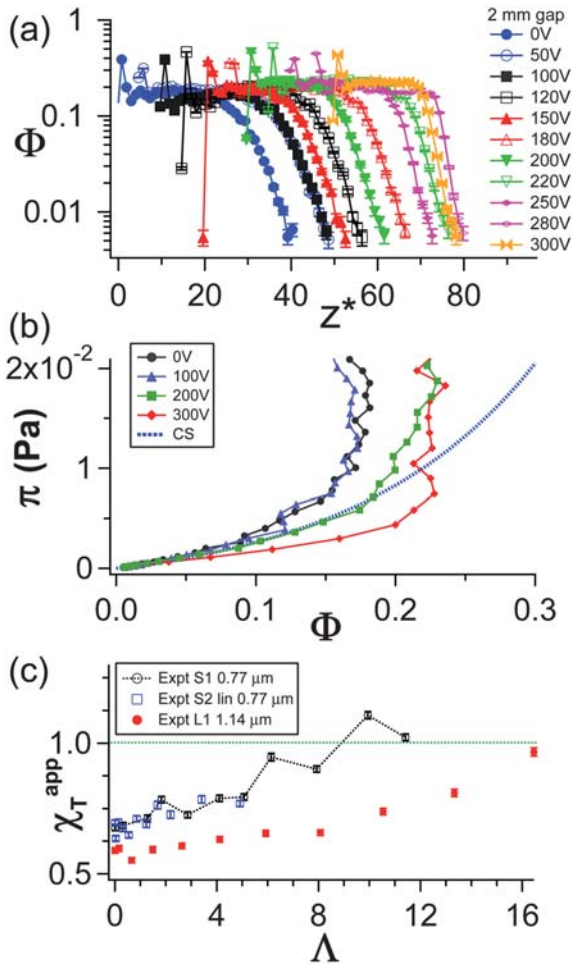

Fig. 2 Colloid sedimentation equilibrium in an external a.c. potential which controls the dipolar strength Λ. (a) Sedimentation profiles φ *vs.* dimensionless height $z^* = z/\sigma$ at increasing voltages (offset to the right from the previous by 0.2 for visual clarity). (b) Equations of state for 4 sedimentation profiles (0 V, 100 V, 200 V, 300 V; only 4 shown for clarity) from (a) are shown in comparison with the Carnahan–Starling relation. (c) The apparent isothermal compressibility χ_T^{app} increases with Λ.

favorable to take a particle from the barometric regime and place it in the denser sediment in the presence of increasing attractions.

For anisotropic interactions, it is clear that even in the limit of weak interactions, the equation of state will not tell the full story, because no information about anisotropy is built into it. Thus we looked next at orientational order parameters.

4 Orientational order parameters

On increasing the electric field, angular correlations between particles increase. This is seen qualitatively in Fig. 3 where increasing field (applied along the vertical direction) gives rise to the increase in orientational order in confocal snapshots at a fixed height. From the 3-dimensional datastacks, two-particle bonds were defined when the distance between two spheres was less than 1.2σ. The bond angular order parameter $\langle\cos^2\theta\rangle$ was then obtained as a function of local volume fraction φ. To improve statistics, several images at a given depth z were averaged. The $\langle\cos^2\theta\rangle$ *vs.* φ profile for 0.77 μm colloids is presented in

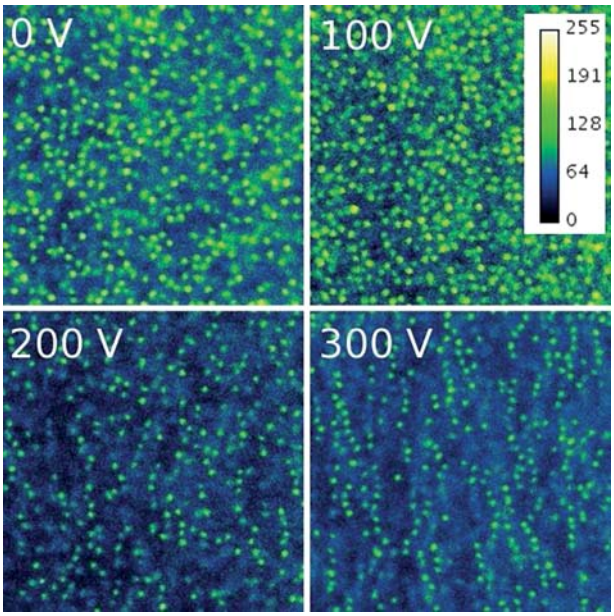

Fig. 3 A comparison of four snapshots at the same height but at 0 V, 100 V, 200 V, and 300 V shows an increase in particle angular correlation with increasing voltage V_o, applied along the vertical direction.

Fig. 4(a). For each value of potential, $\langle\cos^2\theta\rangle$ was roughly constant for $\varphi > 0.02$ (for $\varphi < 0.02$ there are very few bonds and hence the data there is noisy). For an isotropic system in 2 dimensions, one expects $\langle\cos^2\theta\rangle = 0.5$, while for perfectly ordered chains along the field direction, one would obtain $\langle\cos^2\theta\rangle = 1$. In our experiments, for different potentials, the higher potential corresponded to a higher average value of $\langle\cos^2\theta\rangle$, *i.e.* particles are more likely to form chains parallel to the field

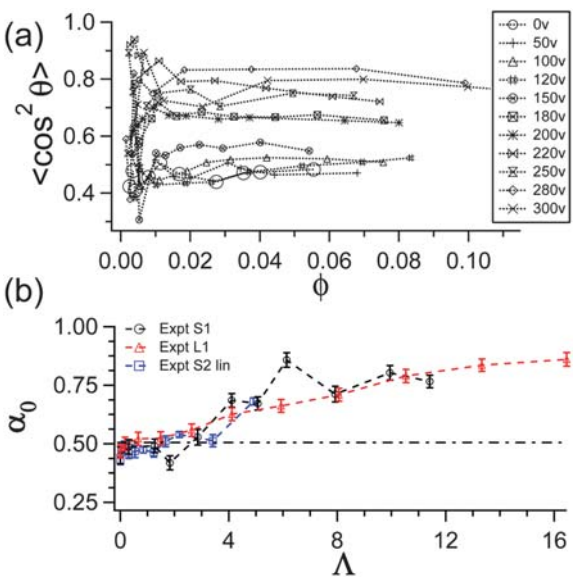

Fig. 4 (a) $\langle\cos^2\theta\rangle$ *vs.* φ profile for $\sigma = 0.77$ μm, for varying potentials and a 2 mm electrode gap. For each potential, $\langle\cos^2\theta\rangle$ was roughly constant for $\varphi > 0.02$, with higher potentials resulted in a higher value. (b) The angular order parameter α_0 is the extrapolated value for $\langle\cos^2\theta\rangle$ at zero packing. α_0 *vs.* Λ for two particle sizes lie on one curve, demonstrating validity of the dipolar interaction for colloids in an electric field.

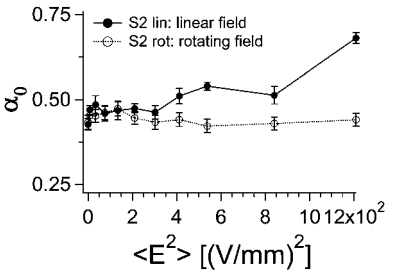

Fig. 5 Low-field response for linear and rotating fields ($\sigma = 0.77$ μm): α_0 *vs.* $\langle E^2 \rangle$. For linear fields, α_0 increases steadily above $\langle E^2 \rangle > 350$ (V/mm)^2. For rotating fields, α_0 is roughly constant, as expected.

direction at higher fields. Since the $\langle \cos^2 \theta \rangle$ *vs.* φ profiles were generally linear for all experiments, we adopted as our orientational order parameter the intercept of linear fit, $\alpha_0 = \langle \cos^2 \theta \rangle|_{\varphi = 0}$.

The dependence of the order parameter α_0 on the dipolar energy parameter Λ is shown in Fig. 4(b). For a perfect particle chain parallel to the linear field, $\alpha_0 = 1$. In our experiments α_0 increased from 0.5 to 0.8 over the range of dipolar strengths probed. For both particle sizes, all data falls on one master curve. Thus the particle-size dependence of the field response scales exactly as one would expect for the dipolar interaction ($\Lambda \propto a^3 E_0^2$). When α_0 is plotted against E_0^2 (not shown) the curves for 1.14 μm spheres ("L1") do not overlay with those for 0.77 μm spheres ("S1" and "S2 lin").

The electric field experiment was repeated in a sample where the electrode geometry allowed the application of either a linear or a rotating electric field (by controlling the relative phase of electrode pairs). We first tested that the linear electric field results were consistent with those in the simpler field geometry (S2 lin and S1 in Fig. 4(b)). We then applied a rotating electric field. Here, α_0 stayed almost steady over the whole range of applied field energy. This is expected because no direction in the x–y plane is preferred in a rotating field. The plot of α_0 *vs.* $\langle E^2 \rangle$ in Fig. 5 shows a clear difference between linear and rotating fields even for relatively small fields.

Colloid sediments with external forces thus display non-trivial behaviour. While there is weaker ordering near the wall than expected from molecular dynamics simulations, the fluid regime can be captured within a hard-sphere-plus-Yukawa (or an effective hard-sphere) model. In spite of the fact that in all cases $\kappa\sigma \gg 1$ for the bulk solution, the observed zero-field behaviour in the sediment corresponds to an effective hard-sphere diameter larger than the bare diameter. In the presence of an external electric field, the dependence of the equations of state for tunable dipolar colloids as a function of dipolar strength has been obtained: the apparent compressibility is found to increase with the dipolar strength parameter Λ. Orientational order parameters prove to be a sensitive probe of anisotropies in colloidal interactions. Colloids in electric fields show dependencies that are indeed quantitatively consistent with dipolar interactions.

Acknowledgements

We acknowledge advice on colloid synthesis from Carlos van Kats, assistance on initial electric field design from Joseph Fitzgerald, and discussions with Amit Agarwal. This work was supported by the Natural Sciences and Engineering Research Council of Canada, the Canada Foundation for Innovation, and ACEnet, with computational support provided by SHARCNET and ACEnet.

References

1 S. Hachisu and K. Takano, *Adv. Colloid Interface Sci.*, 1982, **16**, 233–252.
2 U. Gasser, E. R. Weeks, A. Schofield, P. N. Pusey and D. A. Weitz, *Science*, 2001, **292**, 258–262.
3 P. Wette, H. J. Schope and T. Palberg, *J. Chem. Phys.*, 2005, **123**, 174902.
4 U. Dassanayake, S. Fraden and A. van Blaaderen, *J. Chem. Phys.*, 2000, **112**, 3851–3858.
5 A. Yethiraj, A. Wouterse, B. Groh and A. van Blaaderen, *Phys. Rev. Lett.*, 2004, **92**, 058301–600.
6 A. Yethiraj and A. van Blaaderen, *Nature*, 2003, **421**, 513–517.
7 K. N. Pham, A. M. Peurtas, J. Bergenholtz, S. U. Egelhaaf, A. Moussaid, P. N. Pusey, A. B. Schofield, M. E. Cates, M. Fuchs and W. C. K. Poon, *Science*, 2002, **296**, 104–106.
8 A. Yethiraj, *Soft Matter*, 2007, **3**, 1099–1115.
9 J. E. Martin, E. Venturini, J. Odinek and R. A. Anderson, *Phys. Rev. E: Stat. Phys., Plasmas, Fluids, Relat. Interdiscip. Top.*, 2000, **61**, 2818–2830.
10 A. Agarwal and A. Yethiraj, *Phys. Rev. Lett.*, 2009, **102**, 198301.
11 Z. Tang, N. Kotov and M. Giersig, *Science*, 2002, **297**, 237.
12 M. Stevens and G. Grest, *Phys. Rev. E: Stat. Phys., Plasmas, Fluids, Relat. Interdiscip. Top.*, 1995, **51**, 5976–5983.
13 J. Richardi, M. Pileni and J.-J. Weis, *Phys. Rev. E: Stat., Nonlinear, Soft Matter Phys.*, 2008, **77**, 061510.
14 V. Ballenegger and J.-P. Hansen, *Mol. Phys.*, 2004, **102**, 599–609.
15 M. Mittal, P. Lele, E. Kaler and E. Furst, *J. Chem. Phys.*, 2008, **129**, 064513.
16 R. Piazza, T. Bellini and V. Degiorgio, *Phys. Rev. Lett.*, 1993, **71**, 4267–4270.
17 S.-E. Phan, W. B. Russel, Z. Cheng, J. Zhu, P. M. Chaikin, J. H. Dunsmuir and R. H. Ottewill, *Phys. Rev. E: Stat. Phys., Plasmas, Fluids, Relat. Interdiscip. Top.*, 1996, **54**, 6633–6645.
18 M. A. Rutgers, J. H. Dunsmuir, J.-Z. Xue, W. B. Russel and P. M. Chaikin, *Phys. Rev. B: Condens. Matter*, 1996, **53**, 5043–5046.
19 S. Buzzaccaro, R. Rusconi and R. Piazza, *Phys. Rev. Lett.*, 2007, **99**, 098301.
20 N. H. March and M. P. Tosi, *Liquid State Physics*, World Scientific, 2002.
21 A. van Blaaderen and A. Vrij, *Langmuir*, 1992, **8**, 2921–2931.
22 J. Hoogenboom, P. Vergeer and A. van Blaaderen, *J. Chem. Phys.*, 2003, **119**, 3371–3383.
23 C. P. Royall, J. Dzubiella, M. Schmidt and A. van Blaaderen, *Phys. Rev. Lett.*, 2007, **98**, 188304.
24 T. Biben and J.-P. Hansen, *J. Phys.: Condens. Matter*, 1994, **6**, A345–A349.
25 D. Rapaport, *The art of molecular dynamics simulation*, Cambridge University Press, Cambridge, 2004.
26 T. Voigtmann, A. Puertas and M. Fuchs, *Phys. Rev. E: Stat., Nonlinear, Soft Matter Phys.*, 2004, **70**, 061506.

